A MISSION SYNTHESIS ALGORITHM FOR FATIGUE DAMAGE ANALYSIS

S. Abdullah*, J.A. Giacomin and J.R. Yates

Department of Mechanical Engineering

The University of Sheffield

Mappin Street, Sheffield, S1 3JD

United Kingdom

Abstract

This paper presents a signal processing based algorithm, the Mildly Nonstationary Mission Synthesis (MNMS), which produces a short mission signal from long records of experimental data. The algorithm uses the Discrete Fourier Transform, Orthogonal Wavelet Transform and bump reinsertion procedures. In order to observe the algorithm effectiveness a fatigue damage case study was performed for a vehicle lower suspension arm using signals containing tensile and compressive preloading. The mission synthesis results were compared to the original road data in terms of both the global signal statistics and the fatigue damage variation as a function of compression ratio. Three bump reinsertion methods were used and evaluated. The methods differed in the manner in which bumps (shock events) from different wavelet groups (frequency bands) were synchronised during the reinsertion process. One method, based on time synchronised section reinsertion, produced the best results in terms of mission signal kurtosis, crest factor, root-mean-square level and power spectral density. For improved algorithm performance, bump selection was identified as the main control parameter requiring optimisation.

Keywords: *fatigue, mission, bumps, nonstationary, compression, vehicles*

NOTATION

A	Wavelet scale
A_k	PSD amplitude
B'	Wavelet translation step
b	Fatigue strength exponent
c	Fatigue ductility exponent
CF	Crest factor
D	Fatigue damage for one cycle
E	Modulus of elasticity [MPa]
f	Sampling frequency [Hz]
f_k	Frequency of a harmonic in frequency spectrum [Hz]
Hz	Unit of Frequency expressed in cycles per second.
K	Kurtosis value
N	Number of data points
N_i	Number of cycles with a particular stress range and mean [cycles]
N_f	Number of cycles to failure for a particular stress range and mean [cycles]
RMS	Root-mean-square
$S(f_k)$	Underlying PSD of the Gaussian signal
t	Time [s]
$W_y(a,b)$	Wavelet coefficients for continuous wavelet transform
$W_y(m,n)$	Wavelet coefficients for discrete wavelet transform
x_j	Instantaneous value of the sampled process
$\bar{x}$	Signal mean for a time history
$y(t)$	Fourier synthetic signal
$2N_f$	Reversals to failure
Δf	Frequency interval in frequency domain [Hz]
e_a	Strain amplitude for fatigue time history
e_{max}	Maximum strain for fatigue time history
e_{min}	Minimum strain

e'_f	Fatigue ductility coefficient
l	Skewness of the signal
f_k	Phase angle chosen from a random distribution over the interval 0 to 2π
s_{max}	Maximum stress for fatigue time history [MPa]
s'_f	Fatigue strength coefficient [MPa]
s_m	Mean stress for fatigue time history [MPa]
s_a	Alternating stress for fatigue time history [MPa]
$y(t)$	Wavelets
$y_{a,b}(t)$	Scaled wavelets
y^*	Complex conjugate of y

1. Introduction

Many structural components in vehicles are subject to stochastic loadings and these load histories are often lengthy and random in nature. Random vibration theory has often been introduced in order to analyse and summarise such data. Since fatigue is one of the major causes of vehicle component failure, its life prediction has become a subject of discussion in many texts which treat the subject of random vibration [**1,2**]. Previous research of the subject of fatigue damage calculation has largely concentrated on rainflow cycle counting of the nonstationary signals [**3**], Weibull and Markov approaches [**4**], the strain-life models of Smith-Watson-Topper (SWT) and Morrow, and the linear cumulative damage rule of Palmgren-Miner [**5**]. Fatigue analysis has often been performed using measurements taken from prototype components to predict the fatigue behaviour [**6**]. This is a costly activity because an interactive design cycle is centred on the construction of real prototype components. A more desirable approach involves computer simulation which can be quickly performed during the design cycle in order to achieve the optimal design [**7**]. Since general fatigue loading histories can be lengthy, methods are needed for summarising and reconstructing the time histories. Several previous studies [**8,9**] have shown that nonstationary fatigue time histories can be reconstructed by removing the mean variation so as to produce a stationary signal which can be modelled using the Autoregressive Moving Average (ARMA) approach. Other studies have

researched fatigue editing techniques which reduce the signal length by removing sections of the time histories which cause little damage [**10-13**].

The need to shorten nonstationary time histories for the purpose of mission synthesis has lead to the development of the Mildly Nonstationary Mission Synthesis (MNMS) algorithm first described by Giacomin *et al*. [**14,15**]. This algorithm acts as a compression tool to produce a shortened test sequence from long data records. The algorithm uses the Discrete Fourier Transform (DFT), the Orthogonal Wavelet Transform (OWT) and bump reinsertion procedures. The output mission signals replicate the global statistical parameters of the original signal up to the 4^{th} power, i.e. mean value, variance, skewness and kurtosis. Previous studies performed using road vibration signals [**16,17**] have found that MNMS can achieve mission signals which are up to a factor of 10 shorter than the original data without significant changes in the statistical properties of the signals.

The aim of the research described in this paper was to investigate the effectiveness of the MNMS algorithm in the fatigue analysis application and to develop new modules based on the fatigue damage properties of the individual bump events. In addition to random or pseudo-random background behaviour, many experimentally measured road load data sets encountered when analysing the fatigue life properties of vehicle components contain transient features such as potholes and curb strikes. The extraction and reinsertion of these bumps retains important information which is often lost by conventional strain-life fatigue analysis tools which ignore the load cycle sequence. Consideration of the fatigue damage potential of each individual bump during the operations leading to the shortened mission signal was expected to produce shorter and more accurate sequences. In order to develop and validate the needed procedures, a fatigue analysis case study was performed using experimental data from the lower suspension arm of a vehicle travelling over a pavé surface at 34 km/h. The results suggest that the modified MNMS algorithm produced statistically accurate fatigue missions for compression ratios up to approximately 10 and indicated the areas of greatest parameter sensitivity which should be considered for future development.

2. Theoretical Background

2.1 Classification of Random Time Histories

Random processes can be categorised as stationary or nonstationary. Stationary signals exhibit statistical properties which remain unchanged as a function of time while the statistics of nonstationary signals can be highly dependent on the time of measurement [**18**]. Many signals exhibit time-varying, or nonstationary characteristics, which provide a challenge to analysis and classification using traditional signal processing techniques [**19**]. Examples of nonstationary time histories are presented as Fig. 1. A mildly nonstationary signal can be defined as a random process with stable mean and root-mean-square (RMS) values for most of the record, but with short periods of changed signal statistics due to the presence of transient behaviour.

[INSERT FIG. 1 HERE]

In the MNMS algorithm, global signal statistics are used to evaluate algorithm effectiveness. The statistical parameters considered are the RMS value, kurtosis and crest factor. RMS is the 2nd power statistical parameter which represents the overall energy content of an oscillatory signal. For discrete data sets the RMS value can be approximated by

$$RMS = \left\{ \frac{1}{N} \sum_{j=1}^{N} x_j^{\,2} \right\}^{1/2} \tag{1}$$

where x_j is the instantaneous value of the sampled process $x(t)$ at time $t = j\Delta t$ and N is the number of values in the sampled sequence. Kurtosis is a classical measure of non Gaussian distribution and is highly sensitive to outlying data among the instantaneous values. Kurtosis is the 4th power statistical parameter and for discrete data sets can be approximated by

$$K = \frac{1}{N(RMS)^4} \sum_{j=1}^{N} \left(x_j - \bar{x} \right)^4 \tag{2}$$

For a stationary Gaussian process the kurtosis is approximately 2.9. Kurtosis values higher than 2.9 indicate the existence of numerous extreme values, inconsistent with a Gaussian distribution, while

kurtosis values lower than 2.9 indicate a relatively flat distribution, again inconsistent with a Gaussian distribution. The crest factor is defined as the ratio between a maximum value in the time history and the calculated RMS value:

$$CF = \left| \frac{x_{j\max}}{RMS} \right| \tag{3}$$

The crest factor value for sinusoid time histories is 1.4142 and the value approaches 4.0 in the case of a Gaussian random signal.

2.2 Fatigue Damage Analysis

Fatigue failure is a process that involves crack initiation and propagation of a component under repeated loading. The fatigue behaviour of mechanical components under service loading and its evaluation are usually affected by numerous uncertainties and characterised by several random variables such as materials properties, structural properties and load variation [**20**]. There are three major approaches to predicting fatigue life, namely stress-life, strain-life and fracture mechanics. In general, the stress-life approach is used when the applied stresses are low and below the yield stress of the materials under high-cycle fatigue conditions. The strain-life approach is used when the applied stresses and the local plastic strains are quite large under low-cycle fatigue conditions. A fracture mechanics approach is more appropriate when analysing the fatigue crack propagation under cyclic loading conditions [**21**].

Mean stress can have a substantial effect on fatigue behaviour and in the strain-life approach two mean stress effects models are commonly used, i.e. the Smith-Watson-Topper (SWT) and the Morrow strain-life models. The SWT strain-life model is described by

$$s_{\max} e_a = \frac{\left(s'_f\right)^2}{E} \left(2N_f\right)^{2b} + s'_f e'_f \left(2N_f\right)^{b+c} \tag{4}$$

where E is the material modulus of elasticity, s_{max} is a true maximum stress, e_a is a true strain amplitude, $2N_f$ is the number of reversals to failure, s'_f is a fatigue strength coefficient, b is a fatigue strength exponent, e'_f is a fatigue ductility coefficient and c is a fatigue ductility exponent. The

Morrow's strain-life model is consistent with the observation that mean stress effects are significant at low values of plastic strain and that they have little effect at high plastic strains. Morrow's model is defined by

$$\varepsilon_a = \frac{\sigma'_f}{E}\left(1 - \frac{\sigma_m}{\sigma'_f}\right)(2N_f)^b + \varepsilon'_f (2N_f)^c \tag{5}$$

For loading sequences that are predominantly tensile in nature the SWT approach is recommended. In the case where the loading is predominantly compressive the Morrow approach can be used to provide more accurate life estimates [**5,22**].

The damage caused by each cycle of the repeated loading is calculated by reference to material life curves, such as stress-life (*S*-*N*) or strain-life (*ε*-*N*) curves. N_f value for each cycle can be obtained from Eq. (4) and Eq. (5) for both strain-life models. Fatigue damage, *D*, for one cycle is calculated as

$$D = \frac{1}{N_f} \tag{6}$$

and the total damage caused by *N* cycles is referred to the Palmgren-Miner's rule in which the accumulated damage, *SD*, is expressed as

$$SD = \sum_i \frac{N_i}{N_f} \tag{7}$$

where N_i is the number of actual cycles within a particular stress range and mean, and N_f is the number of cycles to failure for a particular stress range and mean. A fatigue cycle is defined as a closed loop on a cyclic stress-strain curve. The fatigue damage is mainly related to cyclic amplitudes, or ranges, and not to peak values. For uniaxial random loadings rainflow cycle counting is the most commonly used method for predicting the fatigue life of components [**23**].

3. MNMS Fatigue Mission Synthesis Algorithm

Mildly nonstationary signals are characterised by a predominantly random background on which a few large amplitude peaks are superimposed due to short duration transients. A bump can be defined as a large amplitude transient event that may cause the overall time history to deviate locally from a

stationary Gaussian model. A flowchart describing fatigue mission synthesis performed by means of the MNMS algorithm **[13-15]** is shown in Fig. 2.

[INSERT FIG. 2 HERE]

3.1 Signal Processing Elements

The first stage of MNMS processing is the determination of the input signal power spectral density (PSD) so as to quantify its frequency domain characteristics. Each frequency step value of the PSD is characterised by an amplitude value

$$A_k = \sqrt{2\Delta f \cdot S(f_k)} \tag{8}$$

where $S(f_k)$ is the underlying PSD of the Gaussian signal and f_k is the frequency of the harmonic. MNMS then uses the amplitude values A_k were then used to generate a short synthetic Fourier background signal, *y(t),* by means of the Fourier expansion

$$y(t) = \sum_{k=1}^{N} A_k \cos(2pf_k + f_k) \tag{9}$$

where the phase angle f_k is chosen as a random function in the interval from 0 to 2π and the maximum number of samples N is defined by the desired compression ratio. The compression ratio is defined as the ratio between the length in time of the original signal and that of the synthetic Fourier signal.

The next stage of MNMS processing is a wavelet decomposition and wavelet level grouping procedure. A wavelet-based analysis is used due to the superiority of time-frequency methods over Fourier methods when analysing signals containing transient events [**2,24,25**]. Wavelets are analytical functions $y(t)$ which are used to decompose a signal $x(t)$ into scaled wavelet coefficients $W_y(a,b')$. The continuous wavelet transform is a time-scale method that can be expressed as

$$W_y(a,b') = \int_{-\infty}^{\infty} x(t) \frac{1}{\sqrt{a}} y^* \left(\frac{t-b'}{a} \right) dt \tag{10}$$

where $y_{a,b}(t)$ are the scaled wavelets and y^* is the complex conjugate of y. The basis wavelet $y(t)$ can be chosen from a number of functions which satisfy a set of admissibility conditions. A natural extension of continuous analysis is the discretisation of time b' and scale a according to $a = a_0^m$, $b' = na_0^n b_0$ where m and n are integers, $b_0 \neq 0$ is the translation step. This implies the construction of a time-scale grid, and thus a discrete wavelet transform can be defined by

$$W_y(m,n) = \int_{-\infty}^{\infty} x(t) a_0^{-m/2} y^*\left(a_0^{-m}, t - nb_0\right) \mathrm{d}t \qquad (11)$$

When the wavelets $y_{m,n}(t)$ form a set of orthonormal functions there is no redundancy in the analysis, i.e. the procedure can be precisely inverted. The discrete wavelet transform based on such functions is called the Orthogonal Wavelet Transform (OWT).

Of the wavelet basis functions appropriate to forming an orthogonal set, the Daubechies' wavelet was chosen due to its efficiency in providing a large number of vanishing statistical moments. A 12th order representation was adopted due to its successful application in several previous studies involving automotive road data **[26-28]**. Since Daubechies' wavelets of order N provides $\frac{N}{2} - 1$ vanishing moments **[29]**, the 12th order of Daubechies' wavelet can be considered adequate for the MNMS application since greater than two vanishing moments are rarely required when compressing speech or video signals **[30]**.

In MNMS, the OWT is used to split both the original and the synthetic Fourier signals into wavelet levels which consists of the reconstructed signals from the wavelet decomposition for a given value of scale a_0^{-m}. Each wavelet level describes the time behaviour of the signal within a specific frequency band. The number of discrete sampling points in the time history being analysed determines how many wavelet levels can be decomposed. When the number of sampling points N is equal to 2^n ($N = 2^n$), the number of levels obtainable from the OWT decomposition is $n + 1$.

A wavelet grouping stage is used in MNMS to permit the user to group wavelet levels into single regions of significant energy as seen in the PSD plot. Wavelet group time histories are then formed by

the summation of their constituent wavelet level time histories. The wavelet level grouping procedure was developed to avoid situations where energy from one vehicle subsystem resonance concealed data from others. Each of these levels corresponds to a specific frequency range which is physiological to the system being investigated. For many data sets, such as a grouping provides individual frequency bands which completely describe the individual subsystem resonance. In the fatigue analysis implementation of MNMS the wavelet groups were ordered from the lowest frequency to the highest frequency. Fig. 3 presents the wavelet groups chosen in the case of an analysis performed for a 32000 point random vibration signal sampled at 512 Hz measured at the wheel hub of an automobile travelling over a comfort surface at 40 km/h.

[INSERT FIG. 3 HERE]

3.2 Bump Identification and Reinsertion Procedures

In MNMS bump identification is achieved in each wavelet group time history by means of a user selected trigger level which is specific to the wavelet group. Fig. 4a presents a set of possible trigger levels defined in terms of the standard deviation of the data of the individual wavelet group. Once a bump event exceeding the pre-set trigger level is identified, the time extent of the event must be defined. In MNMS bump events have been defined as oscillatory transients having a monotonic decay envelope either side of the peak value. A search identifies the points at which the signal envelope inverts from a decay behaviour. The two inversion points, one on either side of the peak value, define the temporal extent of the bump event as shown in Fig. 4b.

[INSERT FIG. 4 HERE]

Once all bump events have been identified from all wavelet groups they are sorted in descending order from the most severe to the least severe. Using the SWT fatigue damage model the left hand side of Eq. (4) can be seen to consist mainly of constants, thus suggesting that the relative severity can be quantified by means of the product of the maximum strain and the strain amplitude.

$$s_{\max} e_a \approx e_{\max} e_a \approx = e_{\max} \left(\frac{e_{\max} - e_{\min}}{2} \right) \tag{12}$$

In MNMS reinsertion procedures take bumps from a list of events found in the experimental data and reinsert them into the short synthetic Fourier background signal, introducing nonstationary behaviour. Two bump reinsertion procedures are currently defined. In proportional reinsertion the bumps are chosen by moving down the list of sorted bump events in descending steps equal to the compression ratio. This assures that the ratio of the number of bumps that were reinserted to those available is in direct proportion to the overall signal compression ratio. In maximal reinsertion, all the bumps that can fit into the synthetic Fourier signal were reinserted starting from the first event (the one with the highest damage potential) and continuing until there is no further space in the time history. Maximal reinsertion attempts to produce the highest possible kurtosis value, and thus the highest possible nonstationarity and damage potential, using as many as possible of the transient events of the original data set. For large compression ratios, however, not all the bumps from the lowest frequency wavelet group can normally be fit into the Fourier signal due to insufficient space.

When reinserting bump events coming from different wavelet groups, three synchronisation procedures have been defined, i.e. Nonsynchronised, Synchronisation 1 and Synchronisation 2. As shown in Fig. 5a Nonsynchronised reinsertion consists of treating each wavelet group independently, assuming that a bump which occurs in one wavelet group has no relation to any other bump in any other wavelet group. The bumps are reinserted at the point of closest similarity to the data of the wavelet group time history of the synthetic Fourier signal. As shown in Fig. 5b, the Synchronisation 1 procedure reinserts groups of bumps from different wavelet groups which occur simultaneously in time. The wavelet group associated with the lowest frequency band (wavelet group 1) is used as the basis for the synchronisation check. All bumps from wavelet groups 2 and above that are found to occur at the same time as a wavelet group 1 event are clustered together with that bump. These clustered bumps are reinserted into wavelet group 1 of the synthetic Fourier signal at the point of closest similarity. After the clustered bumps are reinserted, the remaining independent bumps are then fitted in the unoccupied space in each of the Fourier wavelet groups. As shown in Fig. 5c, Synchronisation 2 involves reinserting whole segments of the original time history back into the

synthetic Fourier signal. If a bump event is found in any of the wavelet groups, a block of data covering the time extent of the bump feature is taken from the original data set and substituted into the synthetic Fourier signal. This synchronisation strategy, the most conservative, retains all of the original amplitude and phase relationships of the original signal.

[INSERT FIG. 5 HERE]

In order to optimise bump correction each bump event is introduced at a location where the synthetic Fourier signal most closely resembles the transient event. This location is determined by means of a correlation procedure in which the bump event is moved along the time history of the synthetic signal, and the two are compared in terms of the RMS difference at each position. The RMS difference is calculated by

$$RMS_{diff} = \sqrt{\frac{1}{N}\sum_{j=1}^{N}\left(x_j - x_{Fourier,\,j}\right)^2} \tag{13}$$

where N is the number of data points of the bump event. The point in the synthetic Fourier signal where the lowest RMS difference occurs is selected as the insertion point.

4. Vehicle Suspension Arm Case Study

4.1 Experimental Measurements

The effectiveness of the MNMS fatigue algorithm was verified by a case study involving data for a vehicle suspension arm. The signals were experimentally measured on the lower suspension arm of a vehicle travelling at 34 km/h over a Leyland Technical Centre (LTC) pavé durability test track [**31**] shown in Fig. 6a. The signals were measured at the top and side of the suspension arm, the strain gauge locations being shown in Fig. 6b. Two signals were chosen for analysis, one having tensile preloading and the other compressive. Both signals were sampled at 500 Hz for a total of 24000 data points which produced at total record length of 48 seconds. The time histories and power spectral densities of both signals are presented in Fig. 7 and their global signal statistics are presented in Table 1. The kurtosis values suggest mildly nonstationary signal behaviour.

[INSERT FIG. 6 HERE] [INSERT FIG. 7 HERE] [INSERT TABLE 1 HERE]

4.2 MNMS Analysis and Fatigue Damage Calculation

The experimentally measured strain gauge signals were analysed and summarised using MNMS at compression ratios from 1 to 10. Both strain gauge signals were decomposed into 12 wavelet levels and assembled into 4 wavelet groups. Manually selected wavelet group trigger levels in the range from 2.4 to 3.3 standard deviations were found to produce accurate fatigue missions. Fatigue damage was calculated in all cases for both the original experimental data sets and the MNMS generated mission signals using the SWT and Morrow strain-life models as implemented in the nSoft® software package. The material properties given in Table 2 [**22**] were used for the fatigue damage calculation of the vehicle suspension arm which was fabricated from SAE 4340 steel.

[INSERT TABLE 2 HERE]

4.3 Results and Discussions

[INSERT FIG. 8 HERE]

Fig. 7 presents the original experimental time histories and power spectral densities along with typical mission signals obtained using the method of maximum reinsertion, the Synchronisation 2 procedure and a compression ratio of 5. Fig. 8 presents the global RMS, kurtosis and crest factor values of the original data and of the mission signals obtained from MNMS algorithm runs using both reinsertion methods and all three synchronisation methods for compression ratios from 1 to 10. Fig. 8a and 8b presents the RMS values of the original experimental data sets and those of the MNMS fatigue mission signals. The results suggest that the mission signal energy levels accurately matched those of the original data across all compression ratios from 1 to 10.

Fig. 8c presents, for both the tensile and the compressive mean loading conditions, the experimental kurtosis values and those of the fatigue missions obtained for compression ratios from 1 to 10. The mission signal kurtosis was found to be within the range ± 25% with respect to the target experimental value. The kurtosis results of Fig. 8c and 8d suggest that the Synchronisation 2 procedure produced an overcorrection for compression ratios of 3 and greater. For both experimental data sets (tensile and compressive) the mission kurtosis values were higher than those of the experimental target data using both reinsertion methods. The data represents a typical example of the overcorrection that can occur for signals which contain large and frequent transients (bumps). As the quantity and time extent of the transient events present in a signal become a large proportion of the total signal duration, the energy level of the overall signal rises leading to double counting of the energy which finds itself represented in both the synthetic Fourier background and the reinserted segments.

Fig. 8e and 8f present the crest factor values of the original experimental data sets and those of the MNMS fatigue mission signals. The results for the compressive data set are typical of MNMS algorithm results for general signals. In this case the crest factor value is determined by the peak value of the bump having the greatest fatigue damage potential (the first one reinserted by all of the MNMS bump reinsertion schemes) and remains largely unaffected by choice of reinsertion scheme. The exact value is determined by the synchronisation scheme, with the Synchronisation 2 method always providing the greatest value since an actual segment of the road data is reinserted, not a processed representation which might lack energy from one or more wavelet groups. The results for the compressive mean valued signal show greater variation in the crest factor results. This particular data set was characterised by the presence of high energy levels at very low frequencies, a situation which made the crest factor highly dependent on the exact point on the synthetic Fourier time history at which the bump was reinserted. In terms of the synchronisation procedures, Synchronisation 2 produced the crest factor values which were the closest to the target, deviating by 1% to 14% for the tensile mean strain loading and -23% to 13% for the compressive mean strain loading.

Fig. 9 presents the fatigue damage variations for both signals. Fig. 9a and 9c for the case of maximum reinsertion indicate the target damage from the original signal as a straight line and present the fatigue mission damage determined at all compression ratios. In an ideal scenario the concept of maximum

reinsertion might permit the damage to remain constant when most of the original bumps are reinserted into the synthetic Fourier signal. Fig. 9b and 9d present the same quantities for the case of proportional reinsertion, in which the target damage line decreases in proportion to the compression ratio.

[INSERT FIG. 9 HERE]

The Synchronisation 2 method generally produced the highest total fatigue damage distribution compared to other synchronisations for compression ratios greater than 4. The higher fatigue damage potential of the Synchronisation 2 missions is caused by the nature of the signal correction procedure, in which the mission signals preserve fully the original phase and amplitude relationships across the full frequency spectrum of the analysis (all wavelet groups). The damage for all synchronisation procedures decreased when the compression ratio increased. This was caused by the reduction of the number of cycles in the mission signals, a natural result of the signal shortening process as shown in Fig. 10 which plots the number of fatigue cycles obtained using the various synchronisation methods as a function of the compression ratio.

[INSERT FIG. 10 HERE]

For the compressive mean strain signal shown in Fig. 9c and 9d, the Morrow's fatigue damage of the mission signal was often higher than the target. This occurred at compression ratio 1 for maximum reinsertion and for most compression ratios using proportional reinsertion.

Examples of the influence of bump trigger level on the mission synthesis process are provided by the data of Tables 3 and 4. Table 3 presents the number of bump events identified for the tensile mean loading experimental signal and the number reinserted into the synthetic Fourier signal using the Synchronisation 2 procedure. Reducing trigger level produces a proportional increase in the number of bump events identified. For the same experimental signal, Table 4 presents instead the calculated fatigue damage of the mission signals obtained using different bump trigger levels. Damage can be seen to increase with reductions in trigger level (increase in the number of bumps identified and used).

[INSERT TABLE 3 HERE] [INSERT TABLE 4 HERE]

The data of Tables 3 and 4 suggests that the setting of appropriate trigger levels is a critical aspect of the MNMS mission synthesis process, affecting both the signal statistics and the damage potential of the obtained mission signals. When setting the trigger levels during the course of the current study the method of statistical process control **[32]**, as shown in Fig. 11, was considered. The signals were normalised by RMS to produce zero mean ($\bar{x} = 0$) and unity RMS ($s = 1$), and number of data set used in the MNMS analysis, $m = 1$. From the equations in Fig. 11, these values produced $UAL = 3$, $UWL = 2$, $LWL = -2$ and $LAL = -3$. Therefore it was determined that all wavelet groups should be triggered at values of twice the RMS value or greater. The trigger level values used in the current study were also estimated based on previous research [**16,17**] which found optimal trigger level values of 2.0 to 4.5 times the signal RMS for acceleration signals measured for automobiles at the front wheel hub and seat guide. Further support for the trigger levels used comes from fatigue studies [**33,34**] which have suggested that most damage is caused by stress values greater than 2 to 4 times the RMS value of the complete signal.

[INSERT FIG. 11 HERE]

5. Conclusions

The MNMS algorithm has been enhanced for use in fatigue mission synthesis and this study has focused on the fatigue damage analysis of two data sets containing tensile and compressive mean valued strain data for a lower suspension arm of a road vehicle. Each data set consisted of 24000 data points sampled at 500 Hz for a vehicle travelling over a pavé test surface. The two data sets were analysed and synthesised using all bump synchronisation and bump reinsertion procedures currently available in the MNMS algorithm for compression ratios from 1 to 10.

Using the enhanced MNMS algorithm the global signal statistics and fatigue damage results were found to be more precise in the case of the tensile than of the compressive mean data set. For both data sets all mission RMS values were found to be within the range ± 5% and all crest factor values were found to be within ± 23%. For the kurtosis values, however, the tensile mean strain loading missions were in the range ±25% while the compressive means strain loading missions were in the range from -26% to 217%.

Mission signals obtained using the Synchronisation procedure 2 were found to provide the most accurate global signal statistics for both experimental data sets. The authors suggest that this is the result of maintaining all phase relationships and time durations present in the original data across the full frequency bandwidth of the analysis i.e. across all wavelet levels. Synchronisation procedure 2 was also found to provide the most accurate missions in terms of total fatigue damage.

The results of the current study suggest that trigger level is the most important parameter requiring further investigation, and the aspect of MNMS mission synthesis requiring further automation. Analysis of the global statistical properties (RMS, kurtosis and crest factor) and of the fatigue damage produced by the synthesised mission signals suggests that the growth in damage is proportional to, but not linear in, the trigger level value. Further research is required to produce an automated procedure for setting the trigger level of each wavelet group directly fom the statistics of the signal being synthesised. Besides expected time savings, such a procedure should lead to more repeatable and accurate results when working with new and unfamiliar data.

Acknowledgement

The authors wish to express their gratitude to Dr. A. Steinwolf, Dr. W.J. Staszewski and Mr. J. Grainger for their contributions to the previous development of the MNMS algorithm. Thanks are also to Dr. P.Wilkinson of the Leyland Technical Centre (LTC) for his assistance in providing vehicle data measured over LTC test surfaces. Finally, many thanks to Universiti Kebangsaan Malaysia (UKM) and the Malaysian Government for their support.

References

1 **Crandall, S.H.** and **Mark, W.D.**, *Random Vibration in Mechanical Systems,* Academic Press, New York USA, 1973.

2 **Newland, D.E.**, *An Introduction to Random Vibrations, Spectral and Wavelet Analysis*, 3rd Edition, Longman Scientific and Technical, Essex UK, 1993.

3 **Jiao, G.**, A theoretical model for the prediction of fatigue under combined Gaussian and impact loads, *International Journal of Fatigue*, 1995, **17**(3), 215-219.

4 **Tovo, R.**, A damage-based evaluation of probability density distribution for rain-flow ranges from random processes, *International Journal of Fatigue*, 2000, **22**, 425-429.

5 **Dowling N.E.**, *Mechanical Behaviour of Materials: Engineering Methods for Deformation, Fracture and Fatigue,* Second Edition, Prentice Hall, New Jersey, 1998.

6 **Bishop, N.W.M.** and **Sherratt, F.**, *Finite Element Based Fatigue Calculations,* NAFEMS: The International Association for the Engineering Analysis Community, Farnham UK, 2000.

7 **Halfpenny, A.**, A conceptual introduction to fatigue, paper presented at *Altair User Conference*, United Kingdom, 2000.

8 **Leser, C., Thangjitham, S.** and **Dowling, N.E.**, Modelling of random vehicle loading histories for fatigue analysis, *International Journal of Vehicle Design*, 1994, **15**(3/4/5), 467-483.

9 **Thangjitham, S., Dowling, N.E.** and **Leser, C.**, Random fatigue load history reconstruction, *SAE940247 SAE Technical Paper Series,* technical paper presented at International Congress and Exposition, 1994, Feb 28 - March 3, Detroit USA.

10 **Haiba, M., Barton, D.C., Brooks, P.C.** and **Levesley, M.C.,** Can fatigue editing strategies be implemented within a structural optimisation algorithm based on fatigue life?, *The Proc. of the 3rd ASMO UK / ISSMO Conference*, 2001, 9-10th July, Harrogate UK.

11 **Haiba, M., Barton, D.C., Brooks, P.C.** and **Levesley, M.C.,** Review of life assessment techniques applied to dynamically loaded automotive components, *Computers and Structures Journal*, 2002, **80**, 481-494.

12 **Stephens, R.I., Dindinger, P.M.** and **Gunger, J.E.**, Fatigue damage editing for accelerated durability testing using strain range and SWT parameter criteria, *International Journal of Fatigue*, 1997, **19**, 599-606.

13 **Oh, C-S.**, Application of wavelet transform in fatigue history editing, *International Journal of Fatigue*, 2001, **23**, 241-250.

14 **Giacomin, J., Steinwolf, A.** and **Staszewski, W.J.**, A vibration mission synthesis algorithm for mildly nonstationary road data, *ATA 6th Int. Conf. on the New Role of Experimentation in the Modern Automotive Product Development Process*, 1999, 17-19 Nov., Florence, Italy.

15 **Giacomin, J., Steinwolf, A.** and **Staszewski, W.J.**, An algorithm for Mildly Nonstationary Mission Synthesis (MNMS), *Engineering Integrity*, 2000, **7**(January), 44-56.

16 **Giacomin, J., Steinwolf, A.** and **Staszewski, W.J.**, Application of Mildly Nonstationary Mission Synthesis (MNMS) to Automotive Road Data, *ATA 7th Int. Conf. on the Role of Experimentation in the Modern Automotive Product Development Process*, 2001, 23-25 May, Florence, Italy.

17 **Grainger, J.J.**, *Application of Mildly Nonstationary Mission Synthesis (MNMS) to Maserati Wheel Hub Road Data*, M.Eng Thesis, Department of Mechanical Engineering, The University of Sheffield, United Kingdom, 2001.

18 **Bendat, J.S.** and **Piersol, A.G.**, *Random Data: Analysis and Measurement Procedures*, Wiley-Interscience, New York, 1971.

19 **Tacer, B.** and **Loughlin, P.J.**, Nonstationary signal classification using the joint moments of time-frequency distributions, *Pattern Recognition*, 1998, **31**(11), 1635-1641.

20 **Svensson, T.**, Prediction uncertainties at variable amplitude fatigue, *International Journal of Fatigue*, 1997, **17**(Suppl.1), 295-302.

21 **Pan, J.** and **Nicholas, T.**, Effects of mean stresses on multiaxial fatigue life prediction based on fracture mechanics, *International Journal of Fatigue*, 2001, **23**(Suppl.1), S87-S92.

22 nSoft User Manual, *nSoft V5.3 Online Documentation*, nCode International Ltd., Sheffield UK, 2001.

23 **Dowling, N.E.**, Fatigue failure prediction for complicated stress-strain histories, *Journal of Materials*, 1972, **7**, 71-87.

24 **Gu, S., Ni, J.** and **Yuan, J.**, Non-stationary signal analysis and transient machining process condition monitoring, *International Journal of Machine Tools & Manufacture*, 2002, 42, 41-51.

25 **Luo, G.Y., Osypiw, D.** and **Irle, M.**, Vibration modelling with fast Gaussian wavelet algorithm, *Advances in Engineering Software*, 2002, **33**(4), 191-197.

26 **Staszewski, W.J.** and **Giacomin, J.A.**, Application of the wavelet based FRFs to the analysis of nonstationary vehicle data, *Proceedings of the 15th International Modal Analysis Conference*, Orlando, 1997.

27 **Lee, S.K.** and **White, P.R.**, Application of wavelet analysis to the impact harshness of a vehicle, *Proc. Instn Mech. Engrs, Part C, Journal of Mechanical Engineering Science*, 2000, **214**(C11), 1331 – 1338.

28 **Steinwolf, A., Giacomin, J.** and **Staszewski, W.J.**, On the need for bump event correction in vibration test profiles representing road excitations in automobiles, *Proc. of the Instn. of Mech. Engrs, Part D, Journal of Automobile Engineering*, 2002, **216** (D4), 279-295.

29 **Burrus, C.S., Gopinath, R.A.** and **Guo, H.**, *Introduction to Wavelets and Wavelet Transforms: A Primer*, Prentice Hall, New Jersey USA, 1998.

30 **Hubbard, B.B.**, *The World According to Wavelets*, A K Peters, Massachusetts USA, 1996.

31 Leyland Technical Centre (LTC), Aston Way, Leyland, Preston, PR5 3TZ, England.

32 **Oakland, J.S.**, *Statistical Process Control: A Really Practical Guide*, Third Edition, Butterworth-Heinemann, Oxford UK, 1996.

33 **Lambert, R.G.**, Plastic work interaction damage rule applied to narrow-band Gaussian random stress situations, *Journal of Pressure Vessel Technology*, 1998, **110**, 88-90.

34 **Liou, H.Y., Wu, W.F.** and **Shin, C.S.**, A modified model for the estimation of fatigue life derived from random vibration theory, *Probabilistic Engineering Mechanics*, 1999, **14**, 281-288.

Table 1 Global statistics of the vehicle suspension strain signals

Signal Name	GLOBAL STATISTICAL PARAMETERS				PRELOAD CRITERIA
	Global RMS	Global skewness	Global kurtosis	Global crest factor	Global mean shifted
Tensile mean strain loading	7.0	- 0.1	3.4	8.1	15.0
Compressive mean strain loading	19.0	0.1	3.8	4.4	- 48.1

Table 2 Material properties for SAE 4340 steel [**23**]

Ultimate tensile strength, s_u (MPa)	826
Young Modulus, E (MPa)	2.07×10^5
Fatigue strength coefficient, s'_f (MPa)	1232
Fatigue strength exponent, b	-0.1
Fatigue ductility coefficient, e'_f	0.53
Fatigue ductility exponent, c	-0.56

Table 3 Number of bumps and total signal time occupied by bumps obtained at different trigger levels for each wavelet groups in Synchronisation 2

Trigger level				Tensile mean strain loading					
WG1	WG2	WG3	WG4	*NB1*	*t1* (s)	*NB2*	*t2* (s)	*NB3*	*t3* (s)
2.5	3.0	3.6	3.8	16	21.6	15	17.7	8	7.3
2.5	2.8	3.4	3.6	25	22.3	24	19.4	13	5.1
2.4	2.6	3.2	3.4	25	28.0	22	21.9	13	12.0
2.4	2.6	3.0	3.3	30	29.5	24	19.4	15	8.2

Notes:

NB1 = Number of bumps extracted from the original signal at Synchronisation 2 of total time *t1*.

NB2 = Number of bumps reinserted into Fourier background signal (to produce mission signal) at compression ratio 2, maximum reinsertion and Synchronisation 2 of total time *t2*.

NB3 = Number of bumps reinserted into Fourier background signal (to produce mission signal) at compression ratio 2, proportional reinsertion and Synchronisation 2 of total time *t3*.

Table 4 Fatigue damage values at different trigger levels in Synchronisation 2 for tensile strain loading (CR = 2) referring to SWT strain-life model.

Trigger level				Target		Maximum Reinsertion		Proportional Reinsertion	
WG1	WG2	WG3	WG4	*NB1*	*Fatigue Damage per Block (CR = 1)*	*NB2*	*Fatigue Damage / Block*	*NB3*	*Fatigue Damage / Block*
2.5	3.0	3.6	3.8	16	1.36×10^{-5}	15	8.16×10^{-6}	8	8.32×10^{-6}
2.5	2.8	3.4	3.6	25	1.36×10^{-5}	24	8.02×10^{-6}	13	7.75×10^{-6}
2.4	2.6	3.2	3.4	25	1.36×10^{-5}	22	8.03×10^{-6}	13	8.25×10^{-6}
2.4	2.6	3.0	3.3	30	1.36×10^{-5}	24	7.77×10^{-6}	15	6.93×10^{-6}

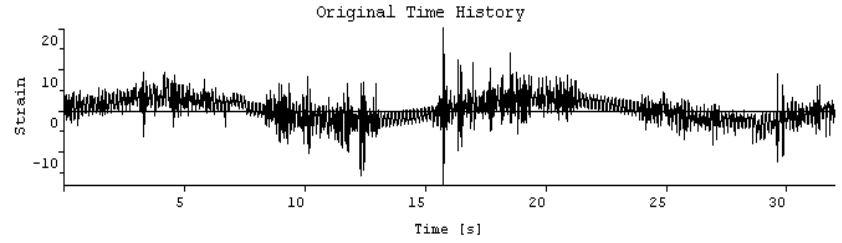

(a)

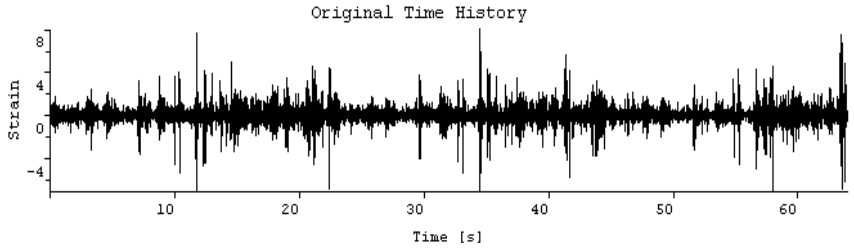

(b)

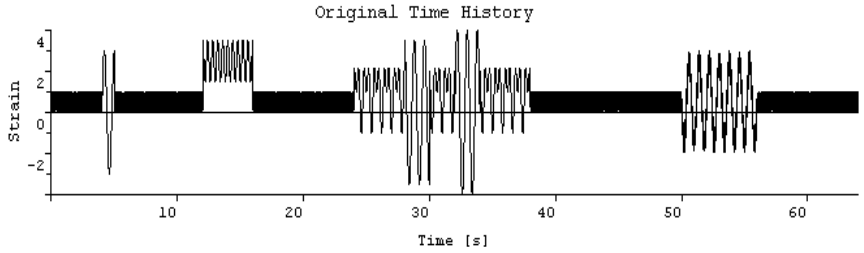

(c)

Fig. 1 Examples of nonstationary time histories: (a) Signal with low frequency background, (b) Zero-mean random signal with shocks, (c) Artificial nonstationary signal with shocks and mean shifts

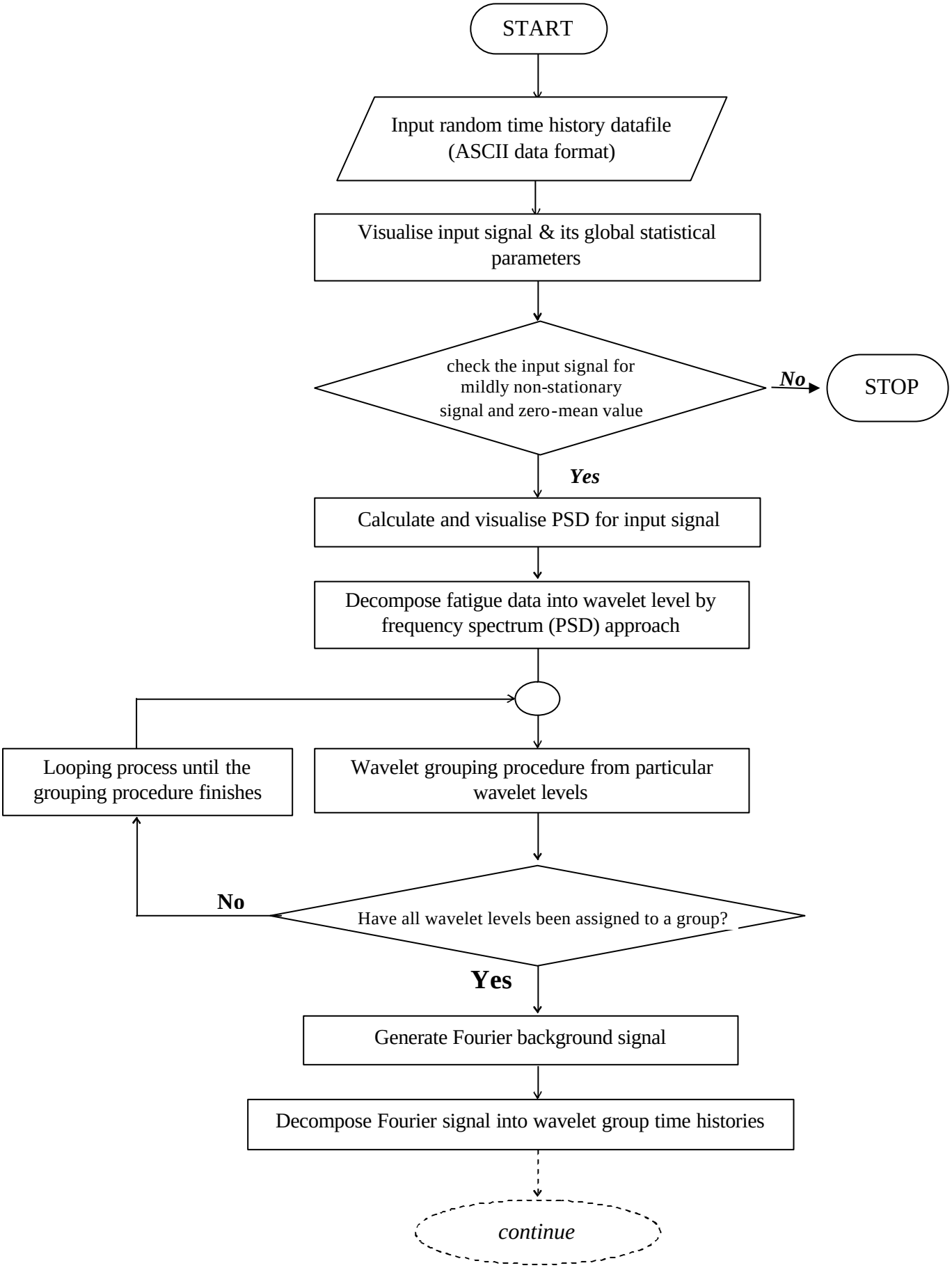
START
Input random time history datafile (ASCII data format)
Visualise input signal & its global statistical parameters
check the input signal for mildly non-stationary signal and zero-mean value
No
STOP
Yes
Calculate and visualise PSD for input signal
Decompose fatigue data into wavelet level by frequency spectrum (PSD) approach
Looping process until the grouping procedure finishes
Wavelet grouping procedure from particular wavelet levels
No
Have all wavelet levels been assigned to a group?
Yes
Generate Fourier background signal
Decompose Fourier signal into wavelet group time histories
continue

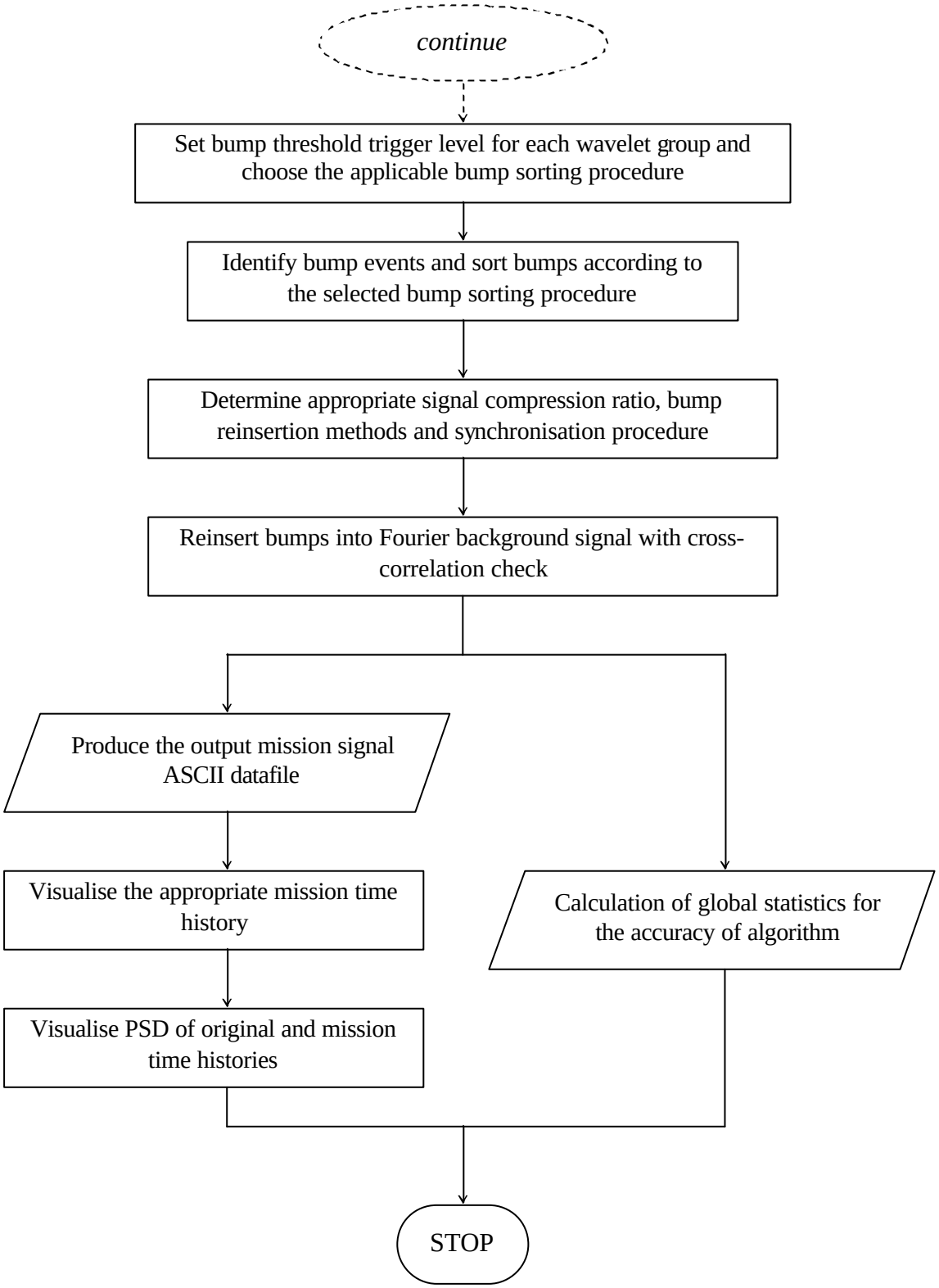

Fig. 2 A flowchart for the fatigue mission synthesis algorithm

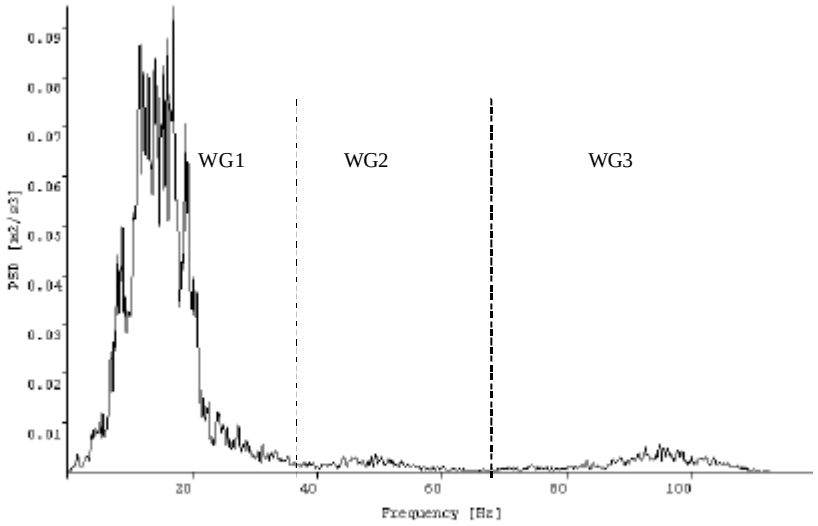

Fig. 3 Frequency distribution (2048 spectral lines) from the wheel hub vertical acceleration time history that has been separated into three wavelet groups

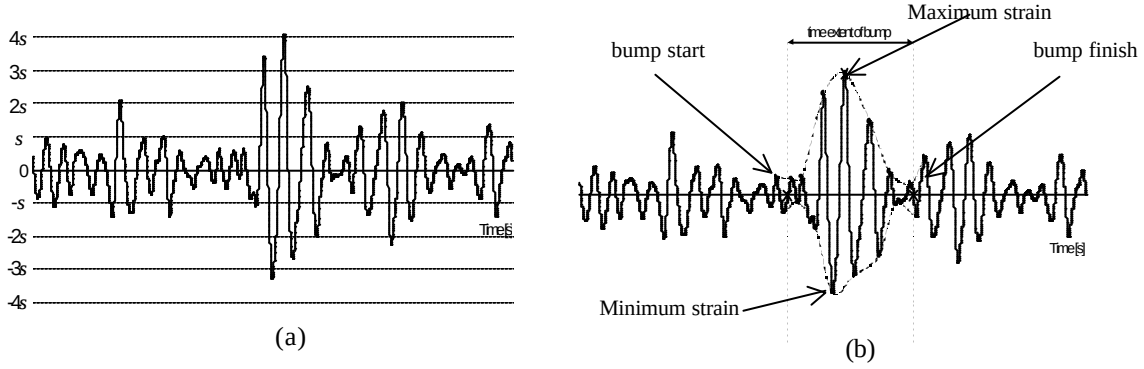

Fig. 4 Bump events identified in the algorithm: (a) Identifying bump events using trigger levels by standard deviation, (b) Decay enveloping of a bump event that showing the bump start, bump finish, maximum and minimum amplitudes

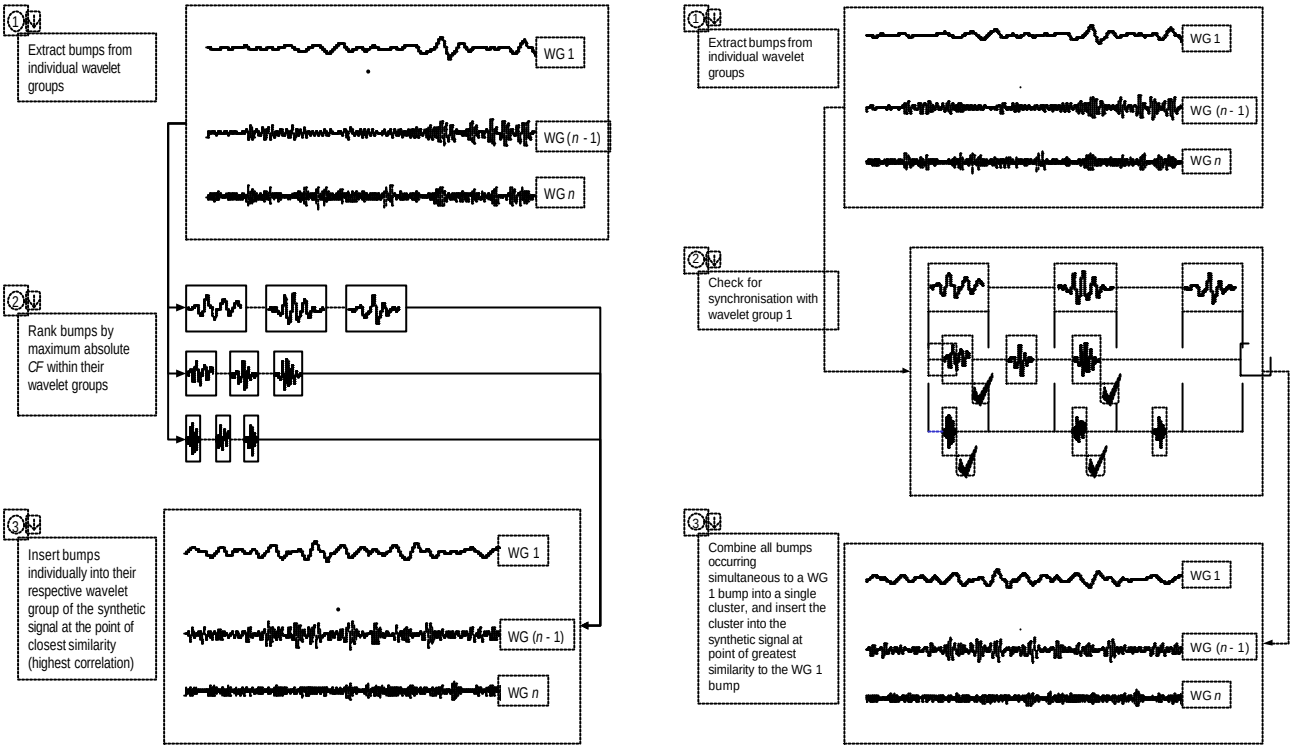

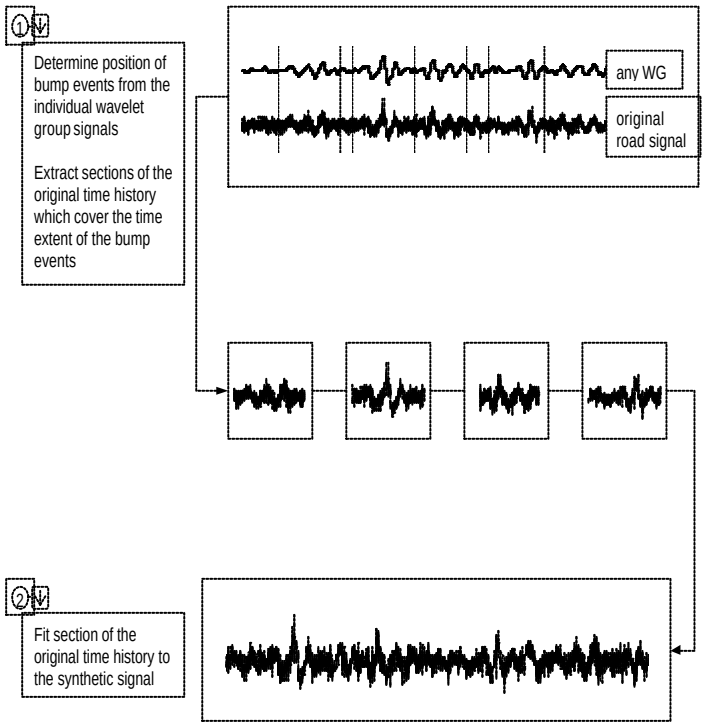

Fig. 5 Schematic diagrams of bump reinsertion procedure: (a) Nonsynchronised, (b) Synchronisation 1, (c) Synchronisation 2

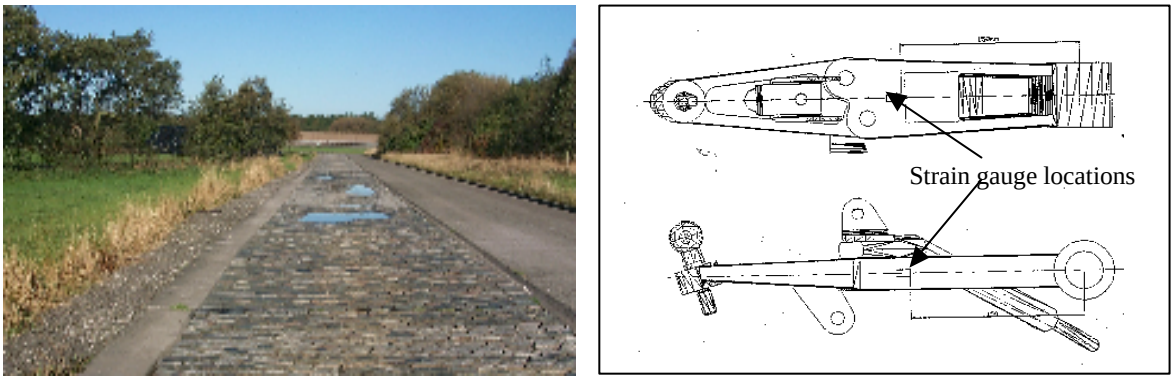

(a) (b)

Fig. 6 (a) Pavé test track used for the road tests, (b) Schematic view of strain gauge locations on the lower suspension arm during the test, top figure is for tensile mean loading and bottom figure is for compressive mean loading [**31**]

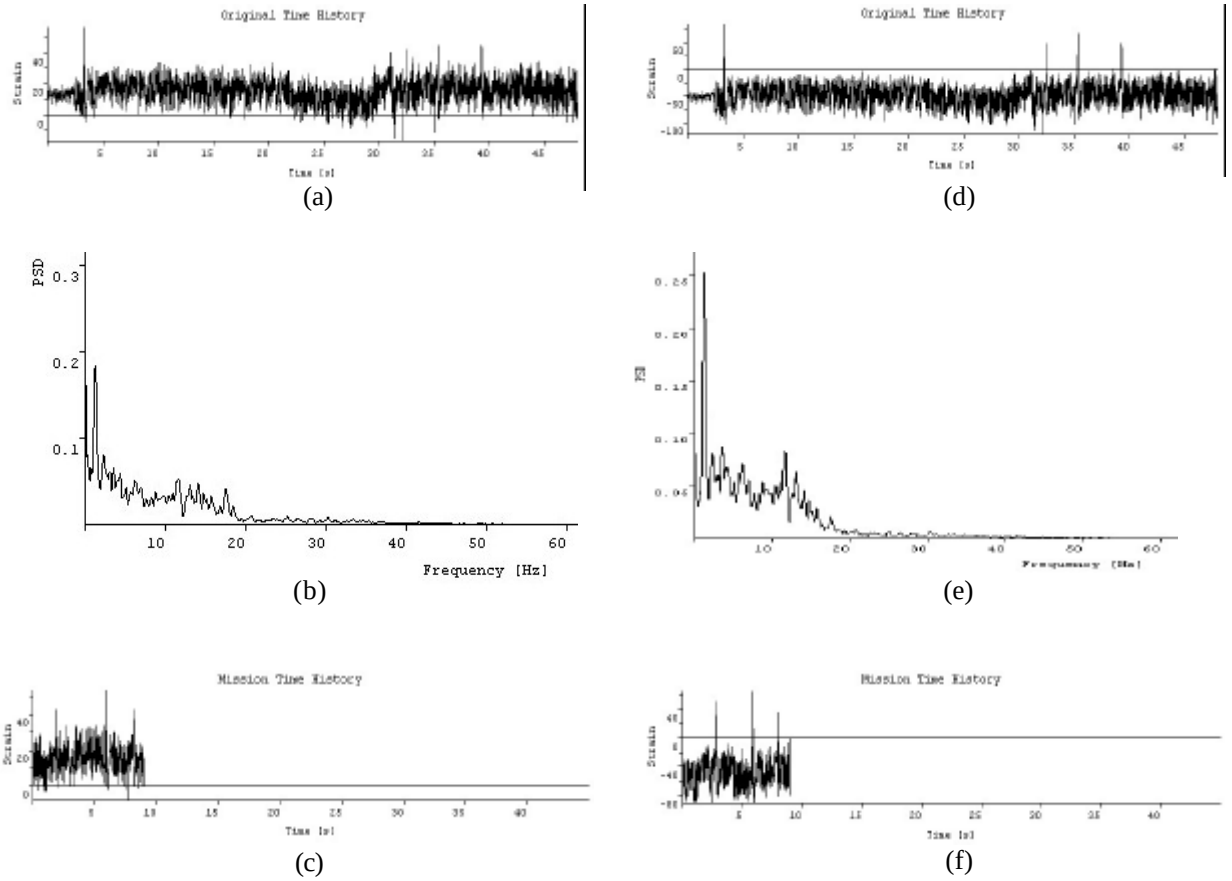

Fig. 7 (a) original time history of tensile mean strain, (b) PSD of tensile mean strain loading, (c) Mission time history of tensile mean strain loading at compression ratio 5, (d) original time history of compressive mean strain loading, (e) PSD of compressive mean strain loading, (f) Mission time history of compressive mean strain loading at compression ratio 5

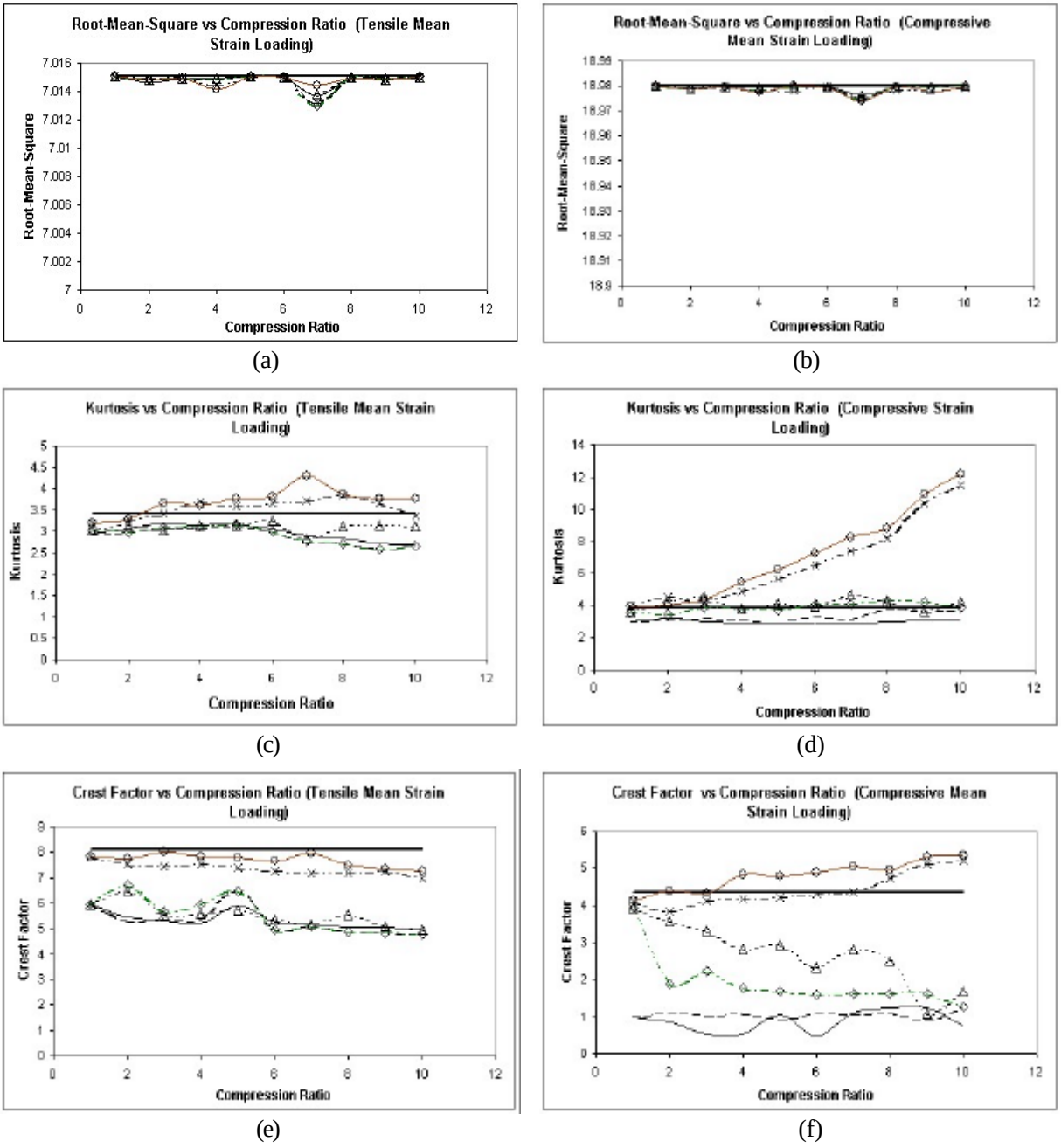

Fig. 8 Signal statistics; (a) RMS for tensile mean strain loading, (b) RMS for compressive mean strain loading, (c) Kurtosis for tensile mean strain loading, (d) Kurtosis for compressive mean strain loading, (e) Crest factor for tensile mean strain loading, (f) Crest factor for compressive mean strain loading

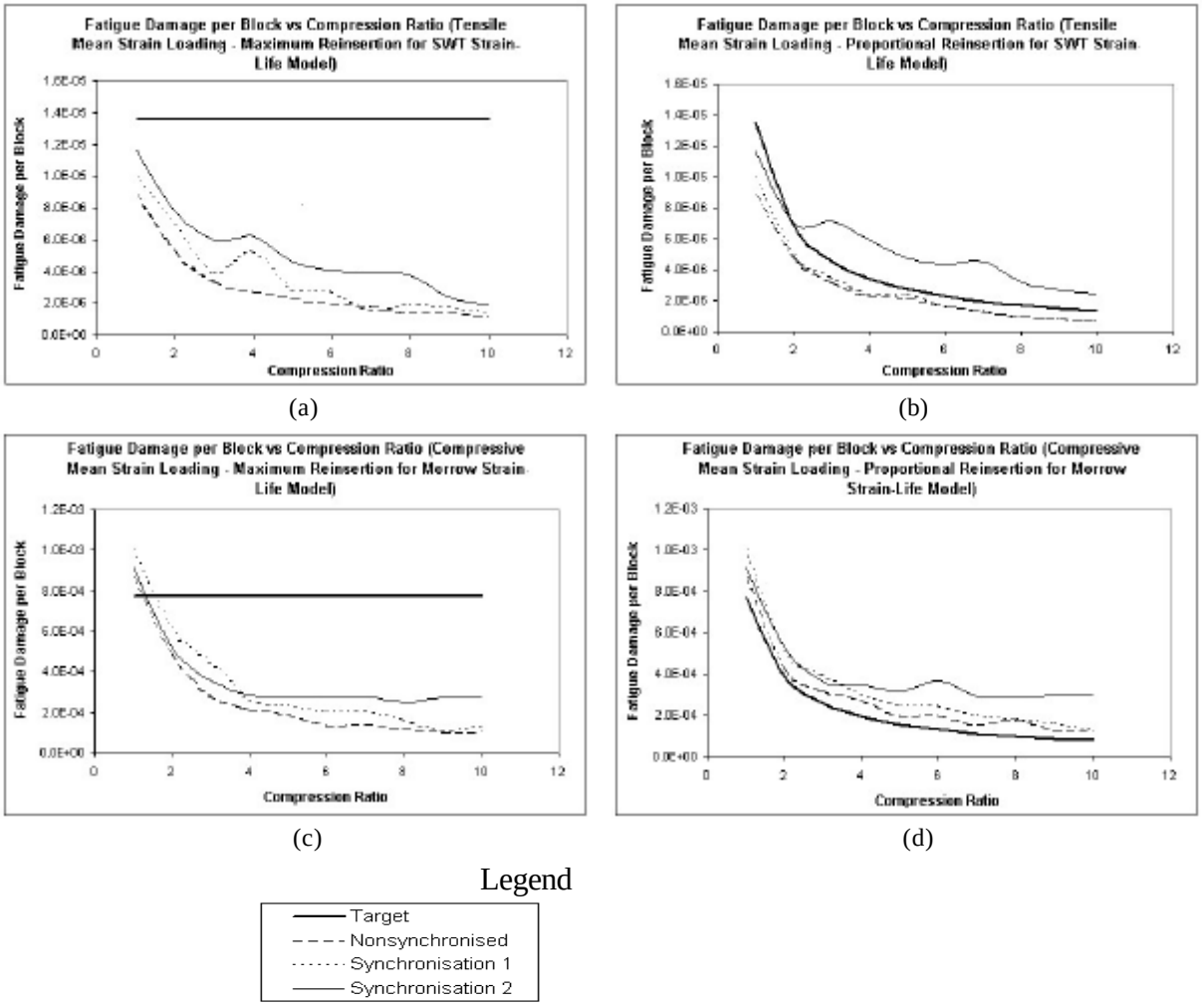

Fig. 9 Results for fatigue damage analysis; (a) Maximum reinsertion for tensile mean strain loading, (b) Proportional reinsertion for tensile mean strain loading, (c) Maximum reinsertion for compressive mean strain loading, (d) Proportional reinsertion for compressive mean strain loading

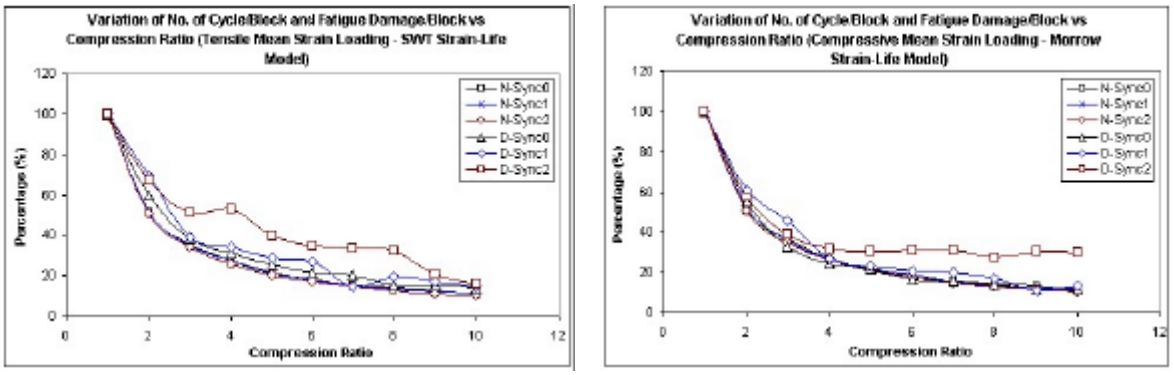

(a) (b)

Legend

N-Sync0 = Number of cycles obtained using Nonsynchronised
D-Sync0 = Fatigue damage obtained using Nonsynchronised
N-Sync1 = Number of cycles obtained using Synchronisation 1
D-Sync1 = Fatigue damage obtained using Synchronisation 1
N-Sync2 = Number of cycles obtained using Synchronisation 2
D-Sync2 = Fatigue damage obtained using Synchronisation 2

Fig. 10 Relationship between fatigue damage and the number of cycles present in the shortened mission signal; (a) SWT strain-life model for tensile mean strain loading signal, (b) Morrow strain-life model for compressive mean strain loading signal

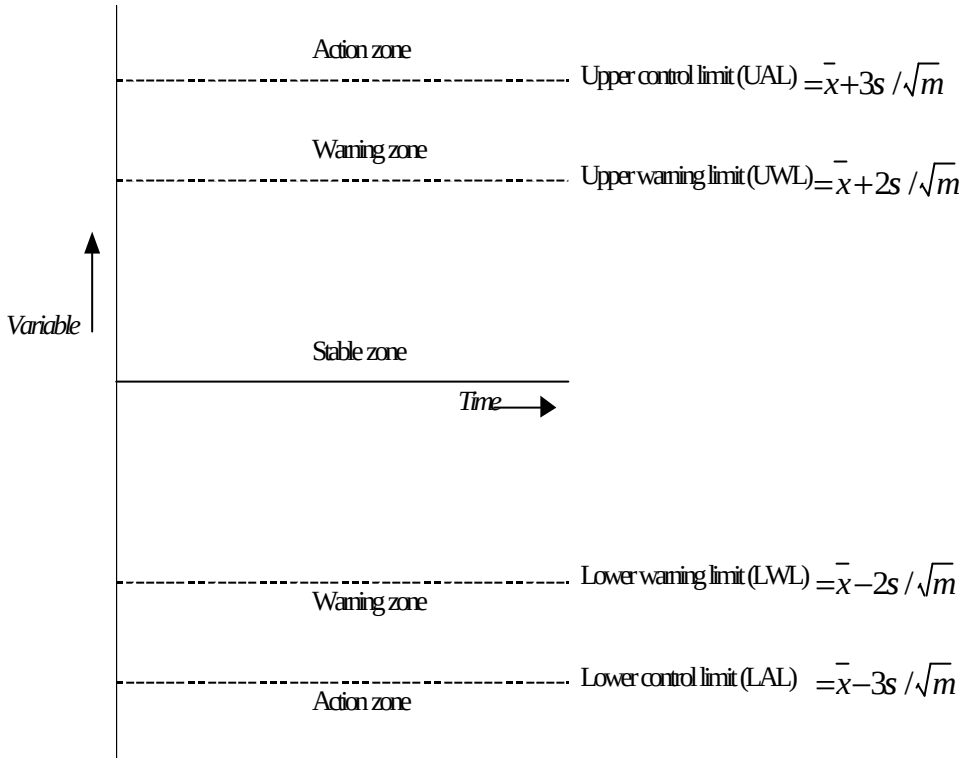

Fig. 11 Schematic diagram of a control chart for the trigger level determination [**32**]